ORNL/TM-2016/536

Scalable Coordination and Control for Multiple Microgrids
Ten Month Progress Report

Alexander M. Melin
Yichen Zhang
Mohammed Olama

September 2016

OAK RIDGE NATIONAL LABORATORY
MANAGED BY UT-BATTELLE FOR THE US DEPARTMENT OF ENERGY

ORNL/TM-2016/536

Electrical and Electronics Systems Research Division

SCALABLE COORDINATION AND CONTROL FOR MULTIPLE MICROGRIDS – TEN MONTH PROGRESS REPORT

Author(s)
Alexander Melin
Yichen Zhang
Mohammed Olama

Date Published: September 2016

Prepared by
OAK RIDGE NATIONAL LABORATORY
Oak Ridge, TN 37831-6283
managed by
UT-Battelle, LLC
for the
US DEPARTMENT OF ENERGY
under contract DE-AC05-00OR22725

CONTENTS

LIST OF FIGURES

ACRONYMS

AC	Alternating Current
CCM	Current Controlled Mode
DC	Direct Current
DECC	Distributed Energy Communication & Control
DER	Distributed Energy Resources
dsMPC	Distributed Stochastic Model Predictive Control
DSO	Distribution System Operator
EM	Expectation Minimization
EMS	Energy Management System
HVAC	Heating Ventilation and Air Conditioning
LDRD	Laboratory Directed Research and Development
LTI	Linear Time Invariant
ML	Maximum Likelihood
MPC	Model Predictive Control
MPPT	Maximum Power Point Tracking
OCV	Open Circuit Voltage
ORNL	Oak Ridge National Laboratory
PCC	Point of Common Coupling
PV	Photovoltaic
SOC	State of Charge
SDE	Stochastic Differential Equation
WT	Wind Turbine

ABSTRACT

The incorporation of distributed energy resources into existing distribution systems provides make voltage and frequency regulation challenging for distribution system operators and in sufficient concentrations can destabilize the power grid. Re-configuring our distribution systems as a system of connected microgrids is one method for mitigating these instabilities. However, there is little economic reason for distribution system operators to undertake this complex upgrade of their systems. By looking beyond voltage, frequency, and power regulation for microgrids, new methods for controlling and operating microgrids can provide new functionality such as load flattening that will benefit distribution systems operators. This report details the initial research into new scalable coordination and control techniques that could be used to add this new functionality.

1. INTRODUCTION

This document is a summary of research into Scalable Coordination and Control for Multiple Microgrids. This work is being performed under the Oak Ridge National Laboratory (ORNL) Laboratory Directed Research and Development (LDRD) program. The goal of this research is to develop new distributed control techniques that will enable multiple microgrids to share resources between themselves to improve functional performance of microgrids in grid tied mode and increase the time that an individual microgrid can operate in island mode. Microgrids are usually designed as a stand-alone system. However, deploying microgrids into distribution networks doesn't make sense with the way that they are currently used. The primary benefit of microgrids is their ability to operate in island mode where they are decoupled from the distribution system. Islanding mode can improve the resilience of a distribution system during rare extreme events. However, when used in a distribution system, the amount of time a microgrid would spend in island mode is very small compared to grid tied operation. To make deployment of microgrids into the distribution network viable, new control functionality needs to be created that will benefit the distribution system operators in grid-tied mode. Fortunately, the distributed nature of microgrid generation and storage means that there are more local sensing, actuation, and computation that can be used to deploy new functionality. For example, with the inclusion of local storage or dispatchable generation, multiple microgrids can be used to reduce variations in total distribution system load which distribution companies can use to reduce the cost of electricity that is purchased from transmission companies.

The two main difficulties in designing coordination and control systems for multiple microgrids are local stochastic generation and the immense number of devices that need to be coordinated. To address these difficulties, techniques from stochastic control and distributed control will be used in the design of the control system. Additionally, predictive models and optimization will be used for long time scale coordination. In section 2., the needed dynamic models of various system components are developed. This includes, power flow, DC to AC inverters, DC to DC converters, wind generation, and solar generation. In section 3., the common definitions for the control system hierarchies used in literature are defined. Section 4. give details of the software implementation of the system models. Section 5. defines the theoretical control framework that will be used for microgrid coordination and control. Finally, in section 6., mathematical definitions of the control objective functions are developed. These objective functions are utilized to optimize the coordinated behavior of the microgrids.

2. SYSTEM COMPONENT MODELS

Model Predictive Control, unlike traditional feedback uses an 'implicit' feedback loop instead of an 'explicit' feedback loop. It solved an *open-loop* optimization at each time step and applies that solution at the same time step, then uses the physical measurements to recalculate the optimal open-loop solution for the next time step. This has the advantage of working well for highly complex nonlinear systems with large uncertainties and stochastic inputs that would be difficult to create stable robust controllers for using other control design techniques that rely on linearity, Gaussian noise, and accurate knowledge of the system dynamics. While MPC deals well with uncertainty, it's deterministic foundation makes it inherently inadequate with systematically dealing with uncertainties. The consequence of this is that it is hard to guarantee the performance of MPC controllers. This inherent inadequacy of MPC controllers has led to the development of stochastic model predictive controllers which can more accurately characterize the uncertainties in the system. This means that accurate models of both the deterministic and stochastic behavior of microgrid components is an essential part of developing a distributed stochastic model predictive control system.

A microgrid is a discrete energy system consisting of distributed energy sources (including demand management, storage, and generation) and loads capable of operating in parallel with, or independently from, the main power grid (Definition by Department of Energy).It is usually made up of **energy harvesters** such as photovoltaic panel (PV) or wind turbine (WT), **energy storages** like battery and their corresponding **power electronics converters**. The energy harvesters and storages can be regarded as sources and the power electronics converters can be regarded as interfaces.

Control of such a complex system is a challenging task mainly because of the following reasons Olivares et al. [2014]:

- **Modelling accuracy**: Three-phase balanced conditions, primarily inductive transmission lines, and constant-power loads are typically valid assumptions in a bulk power system, however, will not hold in microgrids.
- **Low inertia**: Due to the lack of large rotating mass and decouple control of converters, microgrids are usually exposed under low inertia condition thus will have severe frequency deviations under contingency, especially in islanding operation.
- **Uncertainty**: Since power generation in microgrids highly depends on environment condition, generation fluctuates a lot. This makes the power balance be a hard task, especially considering varying load profile. Moreover, parameters and performance of energy harvesters will change due to the environment and operating condition as well.
- **Stability**: Small signal instability will arise due to the improper settings of control gain. Meanwhile, the presence of connected LC filters in parallel and series will lead to resonance.

Besides the stable and optimal operation, more properties and functionalities want to be realized like plug-and-play, harmonics elimination and fluctuation smoothing. These require well-designed control architecture.

Our objective is to design a distributed secondary control for microgrids to eliminate some drawbacks of droop-based primary control and meanwhile enable properties like robustness against model uncertainty,

plug-and-play and renewable fluctuation smoothing. The objective will be achieved through the following subtasks:

(1) Comprehensive modelling of hybrid DC/AC distributed energy resources including harvesters, storages and converters;

(2) Basic control functionality realization such as battery charging/discharging, maximum power point tracking, P/Q and V/f control of DC/AC converter;

(3) Review of state-of-the-art microgrids control schemes;

(4) Power sharing capacity among paralleled connected inverters via droop-based control in islanding microgrids;

(5) Distributed secondary control design considering energy harvesters towards plug-and-play and fluctuation smoothing.

2.1 Source Models

2.1.1 PV Model

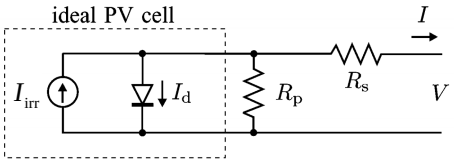

Figure 1. Practical PV device.

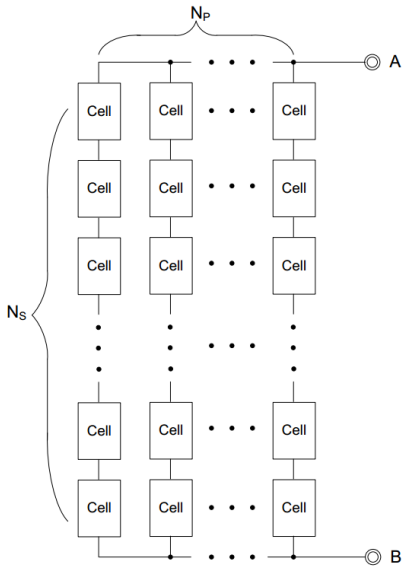

Figure 2. PV cells interconnected in series and parallel Muljadi et al. [2013].

A comprehensive model of PV panel is reviewed in Villalva et al. [2009]. The widely-used PV device model is represented in Fig. 1. The terminal voltage-current relationship is given as:

$$I = I_{\text{irr}} - \underbrace{I_0 \left[\exp\left(\frac{q(V + R_{\text{s}} I)}{akT} \right) - 1 \right]}_{I_{\text{d}}} - \frac{V + R_{\text{s}} I}{R_{\text{p}}} \tag{1}$$

where the diode saturation current I_0 is expressed by

$$I_0 = I_{0,\text{n}} \left(\frac{T_{\text{n}}}{T} \right)^3 \exp\left[\frac{qE_g}{ak} \left(\frac{1}{T_{\text{n}}} - \frac{1}{T} \right) \right] \tag{2}$$

and the light-generated current of the PV cell is expressed by

$$I_{\text{irr}} = (I_{\text{irr,n}} + K_I (T - T_{\text{n}})) \frac{G}{G_{\text{n}}} \tag{3}$$

The parameters are defined as:

$N_s = 54$: Number of series-connected cells
T_{n}[Kelvin] : Nominal temperature
G_{n}[W/m^2] : Nominal irradiation
$I_{\text{sc,n}}$[A] : Nominal short-circuit current
$I_{\text{irr,n}}$[A] : Nominal light-generated current
$V_{\text{oc,n}}$[V] : Nominal open-circuit voltage
$I_{0,\text{n}} \times 10^{-8}$[A] : Nominal diode saturation current
K_V[V/K] : Open-circuit voltage/temperature coeff.
K_I[A/K] : Short-circuit current/temperature coeff.
R_{p}[Ω] : Parallel resistance
R_{s}[Ω] : Series resistance
a : Diode constant
E_g[eV] : Bandgap energy of semiconductor
$q \times 10^{-19}$[C] : Electron charge
$k \times 10^{-23}$[J/K] : Boltzmann constant

If the PV cells are connected in series and parallel to form a PV power station (also called solar park)as shown in Fig. 2, the model is scaled as Muljadi et al. [2013]:

$$\begin{aligned} I_A =& N_{\text{p}} I_{\text{irr}} - N_{\text{p}} I_0 \left[\exp\left(\frac{q(V_A + \frac{N_{\text{s}}}{N_{\text{p}}} R_{\text{s}} I)}{N_{\text{s}} akT} \right) - 1 \right] \\ & - \frac{V_A + \frac{N_{\text{s}}}{N_{\text{p}}} R_{\text{s}} I}{\frac{N_{\text{s}}}{N_{\text{p}}} R_{\text{p}}} \end{aligned} \tag{4}$$

2.1.2 Battery Energy Storage System

The battery model proposed in Tremblay et al. [2007] and Tremblay and Dessaint [2009] has been widely used. Fundamentally modelling the battery is to establish the function of open circuit voltage (OCV) in terms of state-of-charge (SOC). By using different materials, batteries can have different properties as shown in Fig. 3.

Battery	Energy Density (Wh/kg)	Power Density (W/kg)	Cycle Life
Lead-Acid	30-50	100-200	200-300
Lithium-Ion	150-190	300-1500	300-500
Nickel Metal Hydrate	60-120	250-1000	300-500
Zinc Bromide	85-90	300-600	2000

Figure 3. The comparison of properties of different batteries Fu [2013].

Ref. Tremblay and Dessaint [2009] proposes more accurate models to approximate the exponential area as shown in Fig. 4. Based on different materials, four slightly different models are given to represent the four types of batteries: Lead-Acid, Lithium-Ion (Li-Ion), Nickel-Cadmium (NiCd) and Nickel-Metal-Hydride (NiMH). First define variables and parameters:

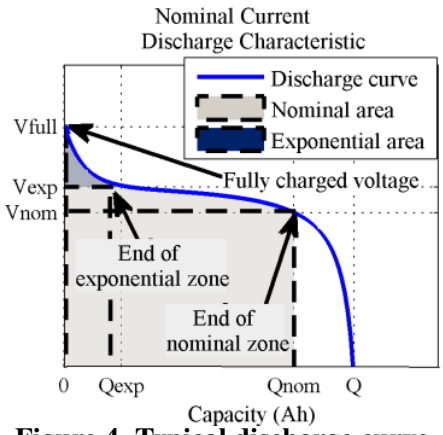

Figure 4. Typical discharge curve.

V_{batt} : Battery terminal voltage [V]

E_0 : Battery constant voltage [V]

K : Polarisation constant [V/Ah] or polarisation resistance [Ω]

Q : Battery capacity [Ah]

$it = \int idt$: Actual battery charge [Ah]

A : Exponential zone amplitude [V]

B : Exponential zone time constant inverse [$(\text{Ah})^{-1}$]

R : Internal resistance [Ω]

i : Battery current [A]

i^* : Filtered current [A]

$Exp(t)$: Exponential zone voltage [V]

$u(t)$: Charge $u(t) = 1$ or discharge $u(t) = 0$ mode

Then hysteresis phenomenon (except for Li-Ion battery) between the charge and the discharge can be represented by a non-linear dynamic system as:

$$\frac{dExp(t)}{dt} = B \cdot |i(t)| \cdot (-Exp(t) + A \cdot u(t)) \tag{5}$$

The mode for Lead-Acid is expressed by
Discharge:

$$V_{\text{batt}} = E_0 - R \cdot i - K\frac{Q}{Q - it}(it + i^*) + Exp(t) \tag{6}$$

Charge:

$$V_{\text{batt}} = E_0 - R \cdot i - K\frac{Q}{it - 0.1Q}i^* - K\frac{Q}{Q - it}it + Exp(t) \tag{7}$$

The mode for Li-Ion is expressed by
Discharge:

$$V_{\text{batt}} = E_0 - R \cdot i - K\frac{Q}{Q - it}(it + i^*) \tag{8}$$

$$+ Ae^{-B \cdot it} \tag{9}$$

Charge:

$$V_{\text{batt}} = E_0 - R \cdot i - K\frac{Q}{it - 0.1Q}i^* - K\frac{Q}{Q - it}it \tag{10}$$

$$+ Ae^{-B \cdot it} \tag{11}$$

The mode for NiMH and NiCd is expressed by
Discharge:

$$V_{\text{batt}} = E_0 - R \cdot i - K\frac{Q}{Q - it}(it + i^*) + Exp(t) \tag{12}$$

Charge:

$$V_{\text{batt}} = E_0 - R\cdot i - K\frac{Q}{|it| - 0.1Q}i^* - K\frac{Q}{Q - it}it + Exp(t) \tag{13}$$

The battery parameters are given in Fig. 5.

Type Parameters	Lead-Acid 12V 7.2Ah	NiCd 1.2V 2.3Ah	Li-Ion 3.3V 2.3Ah	NiMH 1.2V 6.5Ah
$E_0(V)$	12.4659	1.2705	3.366	1.2816
R (Ω)	0.04	0.003	0.01	0.002
K (Ω or $V/(Ah)$)	0.047	0.0037	0.0076	0.0014
A (V)	0.83	0.127	0.26422	0.111
B $(Ah)^{-1}$	125	4.98	26.5487	2.3077

Figure 5. Battery parameters.

2.2 Model of Hybrid DC/AC Distributed Energy Resources

2.2.1 Averaged-Switch Converter Model

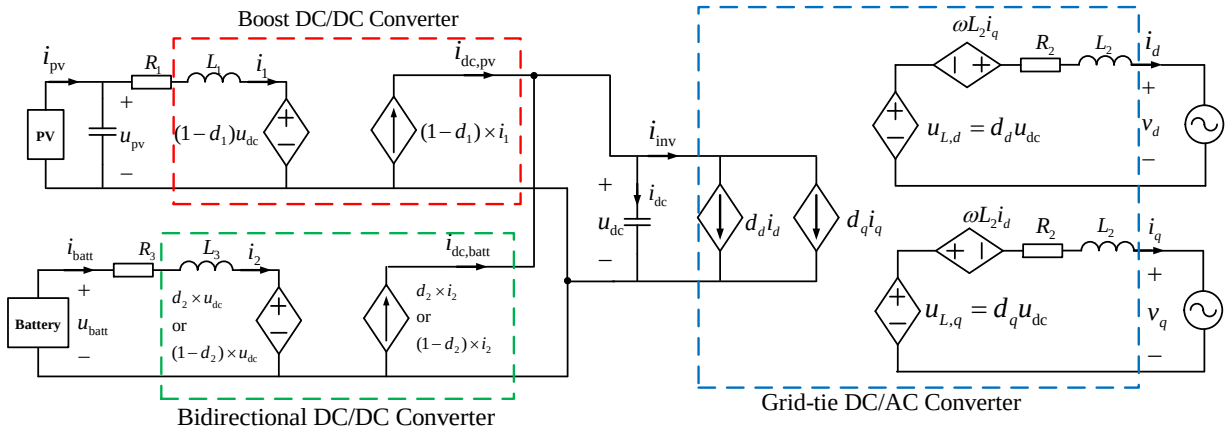

Figure 6. A hybird DC/AC DER in grid-tie mode.

The averaged-switch model is adequate to study the dynamic features of microgrid and thus employed in this project. A very general structure of a converter is given in Figure 7. The main effort is to establish the input-output relationships of the power electronic switch networks in terms of the duty cycle $d(t)$. To achieve this goal, the dynamic states in both LTI networks and switch networks are averaged in a duty cycle.

The switch network of a boost converter is shown in Fig. 8 (a). The averaged mathematical relationship is given as:

$$u_1(t) = d(t)u_2(t) \tag{14}$$

$$i_2(t) = d(t)i_1(t) \tag{15}$$

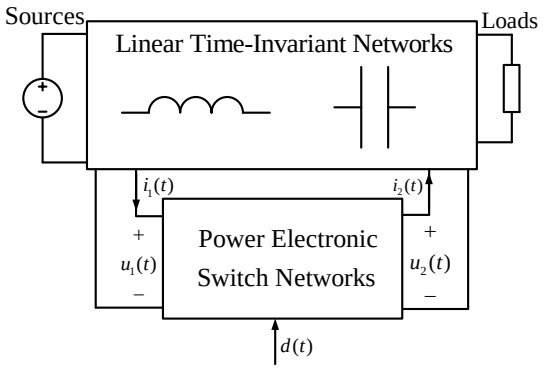

Figure 7. General separate structure of a converter.

Similarly, the switch network of a buck converter is shown in Fig. 8 (b) and its corresponding relationship is expressed as

$$u_2(t) = d(t)u_1(t) \tag{16}$$

$$i_1(t) = d(t)i_2(t) \tag{17}$$

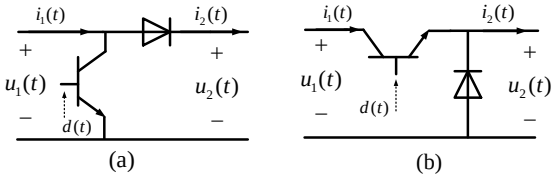

Figure 8. Switch network of a DC converter: (a) Boost type, (b) Buck type.

The topology of three-phase DC/AC converter with a LC filter is presented in Figure 9. The switch network is highlighted in the mesh block. The three-phase voltage $u_{L,abc}$ is controlled to achieve current-controlled mode (CCM). In Blasko and Kaura [1997] a pair of new variables d_d and d_q, which is the equivalent duty cycle in dq frame, is introduced such that the relationship between dc side voltage u_{dc} and ac side voltage in dq frame $u_{L,d}$ and $u_{L,q}$ can be established as follows:

$$u_{L,d}(t) = d_d(t)u_{\mathrm{dc}}(t) \tag{18}$$

$$u_{L,q}(t) = d_q(t)u_{\mathrm{dc}}(t) \tag{19}$$

$$i_{\mathrm{inv}}(t) = d_d(t)i_{L,d}(t) + d_q(t)i_{L,q}(t) \tag{20}$$

Having derived the averaged-switch model, a hybrid DC/AC distributed energy resources (DER) model can be built in equivalent circuit fashion by simply adding the inductors and capacitors as follows Liu et al.

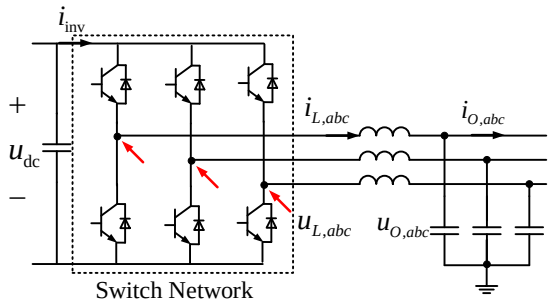

Figure 9. Switch network of a DC/AC converter.

[2011]:

$$C_i \frac{\mathrm{d}u_i}{\mathrm{d}t} = \sum_k i_k \tag{21}$$

$$L_i \frac{\mathrm{d}i_i}{\mathrm{d}t} = u_m - u_n \tag{22}$$

2.2.2 Comprehensive Model and Basic Control of a Hybrid DC/AC DER

Here we illustrate a hybrid DC/AC DER consisting of a PV generator and battery storage system. The comprehensive models represented by equivalent circuits is shown in Figure 6 and Figure 10, respectively. The boost DC/DC converter connected to the PV panel is to achieve maximum power point tracking (MPPT) functionality. The battery is connected to a bidirectional DC/DC converter to realize charging and discharging control meanwhile stabilize the DC link voltage. The converter can run in grid-tie mode and island mode with slightly different equivalent circuit models. In grid-tie mode, the terminal voltage of converter is assumed to be fixed at grid voltage level, while in island mode it is determined by island network power flow. The control of DC/AC converter then operates at P/Q mode and V/f mode, respectively.

In the following context, superscript $*$ denotes the reference value, and bold symbols denote command.

2.2.3 Control Boost DC/DC Converter - MPPT

The control of the boost DC/DC converter is driven by the MPPT algorithm. The inputs are measured PV panel terminal voltage and current. The output is the duty cycle d_1. The perturbation and observation method is the most popular MPPT algorithm and employed in this model. The flow chart of the algorithm can be found in Yafaoui et al. [2007].

2.2.4 Control of Bidirectional DC/DC Converter

The battery charging/discharging control is realized by controlling the bidirectional DC/DC converter. The control loops can be designed to achieve different targets such as different charging algorithms Armstrong

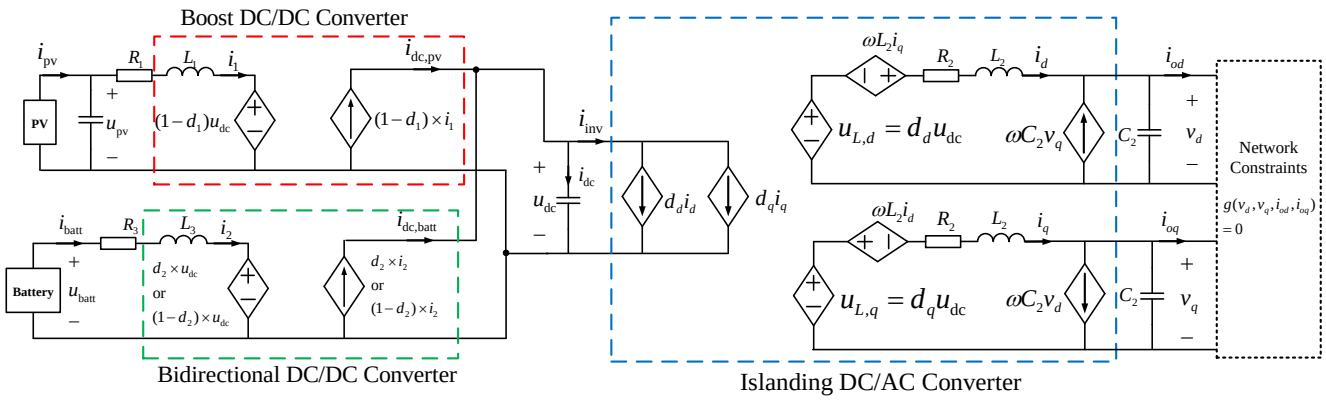

Figure 10. A hybird DC/AC DER in island mode.

et al. [2008], or stabilizing the DC link voltage Wang et al. [2012]. In this system, the latter one is implemented. Under battery discharging situation, where $i_{\text{batt}} > 0$, the DC/DC converter functions as a boost converter, looking from the battery side. When the battery is in the charging process, the converter is working as a buck converter. The steady-state relationships of both converters are given in previous subsections. The standard control loop is represented in Figure 11.

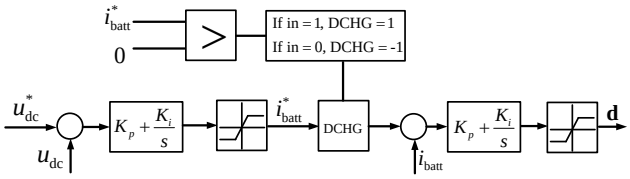

Figure 11. Control of the bidirectional DC/DC converter.

2.2.5 Control of DC/AC Converter in Grid-tie and Island Modes

Depending on their operation in an AC microgrid, the controlled modes of power converters can be classified into **grid-feeding**, **grid-forming** and **grid-supporting** modes Rocabert et al. [2012].

The grid-feeding control is mainly designed to deliver power to an energized grid, also known as P/Q control. The converters under such control can be represented as an ideal current source connected to the grid in parallel with high impedance. In this application, it is important for this current source to be perfectly synchronized with the AC voltage at the connection point, in order to regulate accurately the active and reactive power exchanged with the grid. The simplified scheme of the grid-feeding power converter is depicted in Figure 12. The grid-forming control can be represented as an ideal AC voltage source with a low-output impedance, setting the voltage amplitude E^* and frequency ω^* of the local grid by using a proper control loop, as illustrated in Fig. 1(a).

The grid-supporting converters can be represented either as an ideal AC-controlled current source in parallel with a shunt impedance, or as an ideal AC voltage source in series with a link impedance. Its

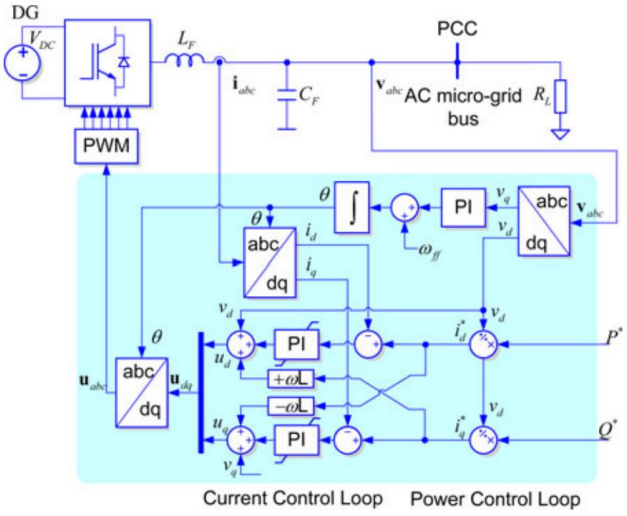

Figure 12. Basic control of a three-phase grid-feeding power converter Rocabert et al. [2012].

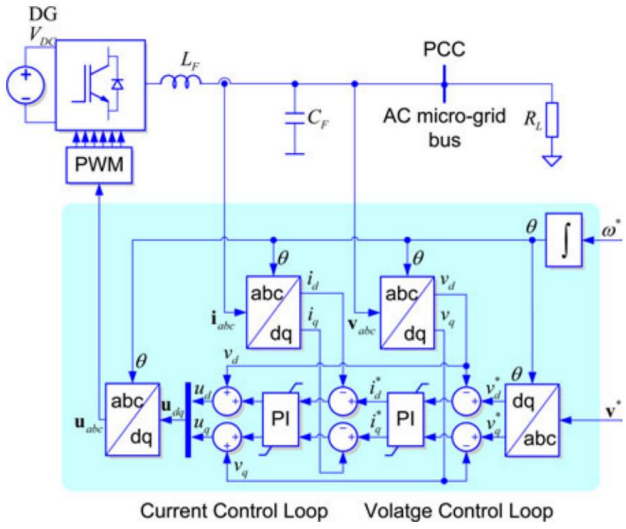

Figure 13. Basic control of a three-phase grid-forming power converter Rocabert et al. [2012].

objective is to deliver proper values of active and reactive power to contribute to the regulation of the grid frequency and the voltage. The most widely used grid-supporting functionality is so-called inertia emulation to enhance the inertia response in a grid with high penetration of renewable sources.

In the above control diagrams, $\mathbf{u}_d$ and $\mathbf{u}_q$ are the control commands set to PWM. To fit the control structure into our averaged-switch model, a simple calculation is needed as follows:

$$\mathbf{d}_d = \frac{\mathbf{u}_d}{u^*_{\text{dc}}} \tag{23}$$

$$\mathbf{d}_q = \frac{\mathbf{u}_q}{u^*_{\text{dc}}} \tag{24}$$

3. CONTROL HIERARCHY IN A MICROGRID

The previous sections have explained models and controls in a single DER point of view, which are the basic context as provision for microgrid analysis and control design. In this section, we are going to review the state-of-the-art microgrid control methods hierarchically and clarify the position of our targets.

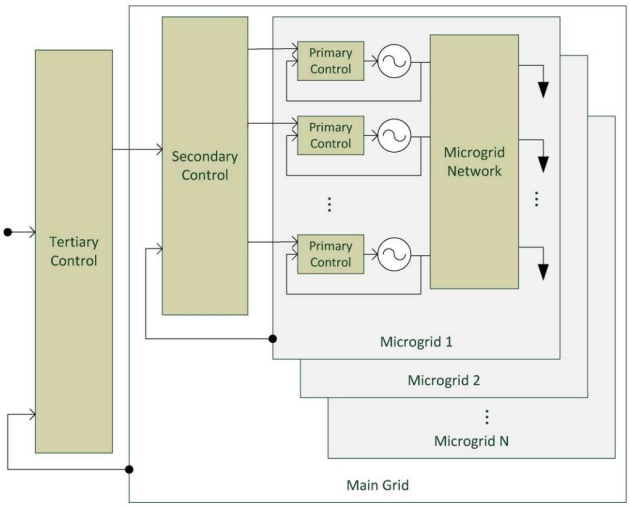

Figure 14. Hierarchical control levels: primary control, secondary control, and tertiary control Olivares et al. [2014].

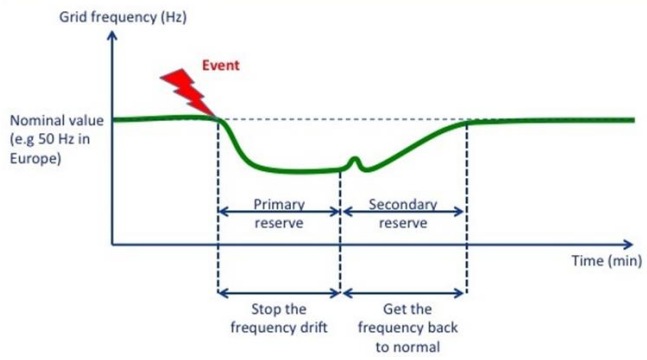

Figure 15. A typical frequency response under primary and secondary control.

Hierarchically speaking, microgrid control can be divided into three levels: **primary** control, **secondary** control and **tertiary** control as shown in Figure 14. Figure 15 has shown a typical frequency response of a system under primary and secondary control, which clearly illustrates the one of responsibilities of primary and secondary control, that is, frequency stabilization and frequency restoration, respectively.

3.1 Primary Control

Primary control, also known as local control or internal control, is the first level in the control hierarchy, featuring the fastest response. This control is based exclusively on local measurements. When the

microgrid is running at grid-tie mode, primary control modes can be either grid-feeding or grid-supporting. When it comes to islanding mode, the primary control is responsible for stabilizing frequency and voltage through proper power sharing schemes as shown in Figure 15. The power sharing schemes can be divided into **communication-based** and **droop characteristic-based** schemes Han et al. [2016].

Communication-based control techniques can achieve excellent voltage regulation and proper power sharing. Moreover, in contrast to droop controllers, the output voltage amplitude and frequency are generally close to their ratings without using a secondary control. It can be realized in either **concentrated**, **master/slave** or **distributed** fashion. However, these control strategies, which require communication lines between the modules, result in increased cost of the system. Long distance communication lines will be easier to get interfered, thus reducing system reliability and expandability.

The droop control can enable proper power sharing among converters without interunit communications. It can avoid complexity and high costs, and improve redundancy and reliability requirements. Most importantly, such a system is easier to expand because of the plug-and-play feature of the modules which allows replacing one unit without stopping the whole system. Therefore, droop control is widely used in industrial application. Droop control is implemented before the grid-forming control loop in Figure 13. The well-known P/Q droop characteristics is expressed as:

$$\omega^* = \omega_0 - m(P_0 - P_{\text{meas}}) \tag{25}$$

$$E^* = E_0 - n(Q_0 - Q_{\text{meas}}) \tag{26}$$

Different from dq voltage and current control in Figure 13, another amplitude and phase control is proposed in Chandorkar et al. [1993] and illustrated in Figure 16 with modified commands as:

$$\mathbf{d}_d = \frac{U_{\text{ref}} \times \cos\delta_p}{u^*_{\text{dc}}} \tag{27}$$

$$\mathbf{d}_q = \frac{U_{\text{ref}} \times \sin\delta_p}{u^*_{\text{dc}}} \tag{28}$$

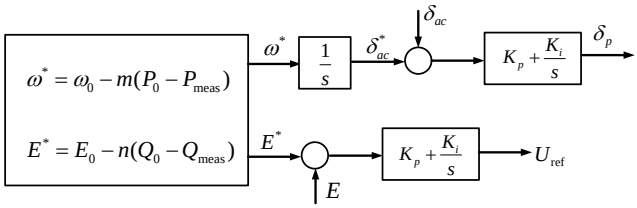

Figure 16. An amplitude and phase control scheme for islanding converter.

However, droop characteristic presents several drawbacks as follows:

(1) Frequency and voltage deviations

(2) Unsuitability for nonlinear loads due to harmonics and ignoring load dynamics

(3) Inability to provide accurate power sharing among DER units due to output impedance uncertainties

(4) Fluctuant and changeable output power of DERs

To overcome these drawbacks, several improved droop control methods have been developed. These methods can be categorised into four groups: 1) conventional and variants of droop control; 2) virtual structure-based methods; 3) construct and compensate-based methods; and 4) hybrid droop/signal-injection-based methods Han et al. [2016].

3.2 Secondary Control

Secondary control, also referred to as the microgrid energy management system (EMS), is the unit in charge of ensuring power quality, mitigating voltage and frequency deviations (as shown in Figure 15), and coordination of the individual DER units for their optimal operation by determining the set points for the primary control Yazdanian and Mehrizi-Sani [2014]. Secondary control can also target to overcome some drawbacks of droop-based primary control. Secondary control is the highest hierarchical level in a microgrid, and operates on a slower time frame as compared to the primary control in order to (1) decouple secondary control from primary control, (2) reduce the communication bandwidth by using sampled measurements of the microgrid variables, and (3) allow enough time to perform complex calculations Olivares et al. [2014].

Secondary control is usually realized as a centralized controller. However, extensive research has been done on design secondary control in a distributed way such that the failure of a single unit will not produce the fail down of the whole system. Under this type of control architecture, every DER has its own local secondary control which will generate proper reference signals for the primary control level. Information will be shared through communication network. A architecture comparison is illustrated in Figure 17. Variety of control schemes have been successfully implemented in microgrid secondary control in a distributed fashion such as distributed model predictive control (MPC), consensus-based techniques, agent-based techniques and decomposition-based techniques Yazdanian and Mehrizi-Sani [2014].

3.3 Tertiary Control

The scope of tertiary control is not only in a single microgrid, but among several microgrids and the host grid as shown in Figure 14. Tertiary control is responsible for coordinating the operation of multiple microgrids interacting with one another in the system, and achieving economic optimization based on energy prices and electricity market. Information is exchanged with the distribution system operator (DSO). Thus tertiary control can be considered part of the host grid, and not the microgrid itself.

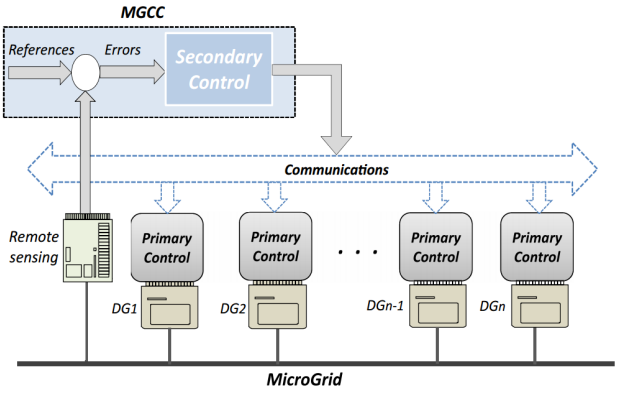

(a)

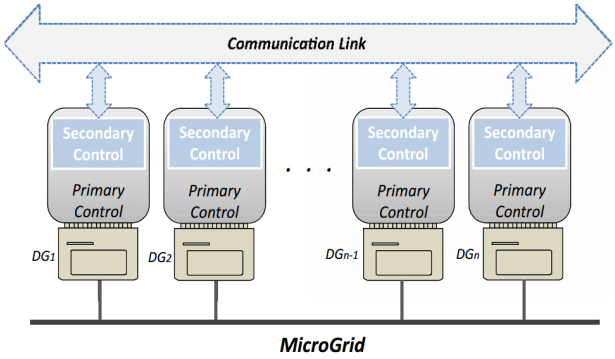

(b)

Figure 17. Secondary control architecture: (a) Centralized control, (b) Distributed Control Shafiee et al. [2014].

4. IMPLEMENTATION

Based on the previous models that we have derived, a purely mathematical model of a hybrid DC/AC DER with P/Q and V/f control has been established in SIMULINK. Every branch detail can be checked. By connecting with a load, this model become a basic DC/AC hybrid microgrid, which can operate under grid-tie mode and islanding mode. The overall model is shown in Figure 18.

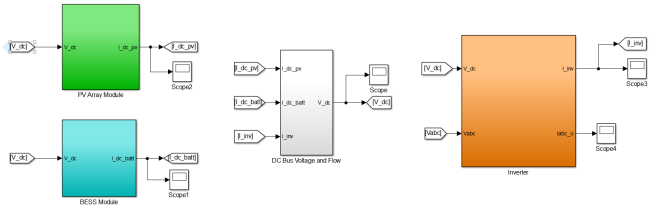

Figure 18. A simple hybrid DC/AC microgrid simulation model in SIMULINK.

The current flow represent the energy exchange as follows:

$$C\frac{\mathrm{d}u_{\mathrm{dc}}}{\mathrm{d}t} = i_{\mathrm{dc,pv}} + i_{\mathrm{dc,batt}} - i_{\mathrm{inv}} \tag{29}$$

Since we assume ideal switch, the power exchange in the inverter is expressed as:

$$u_{\mathrm{dc}} i_{\mathrm{inv}} = \frac{3}{2}(u_d i_d + u_q i_q) \tag{30}$$

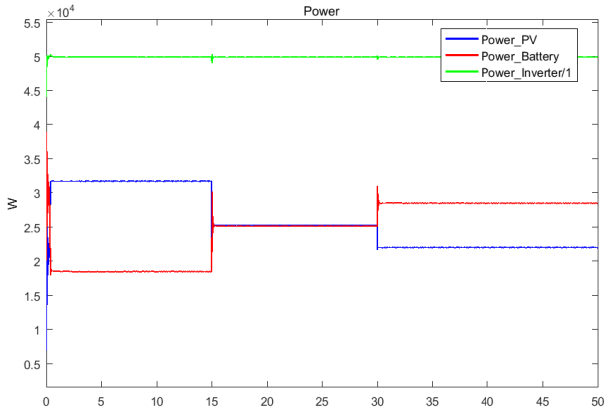

Figure 19. Power exchange in the system.

First let the system operate under grid-tie mode and assume two abrupt changes of solar irradiance: 1000 W/m^2 to 800 W/m^2 at 15 s and 800 W/m^2 to 700 W/m^2 at 30 s. The simulation results are plotted in the following figures. The inverter power control command is set at 50 kW. The battery works at discharging mode to compensate the power demand under different solar irradiance conditions. The DC link voltage can be regulated within 0.3 s.

When the system operates at islanding condition, the same disturbance of solar irradiance is assumed. Droop control is equipped to stabilize grid frequency and voltage. The simulation results are presented in

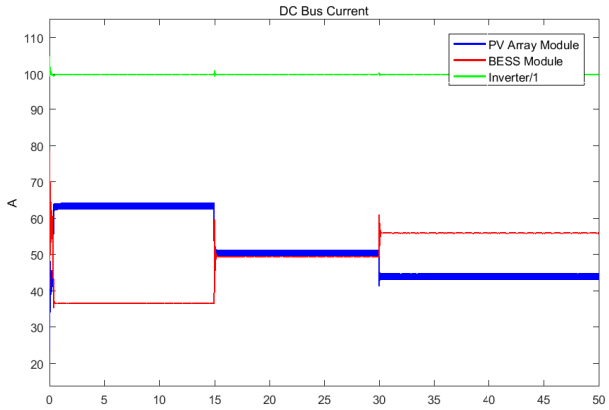

Figure 20. DC link current flows.

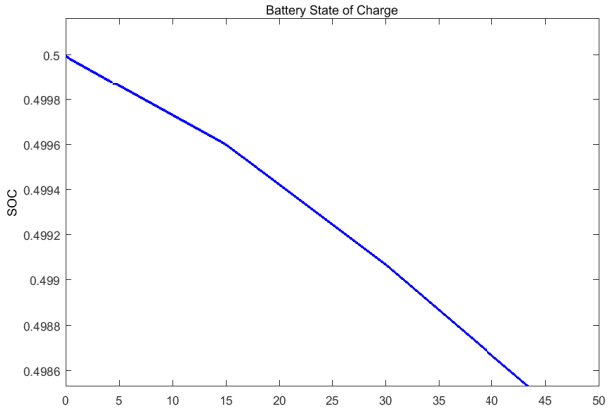

Figure 21. Battery state of charge.

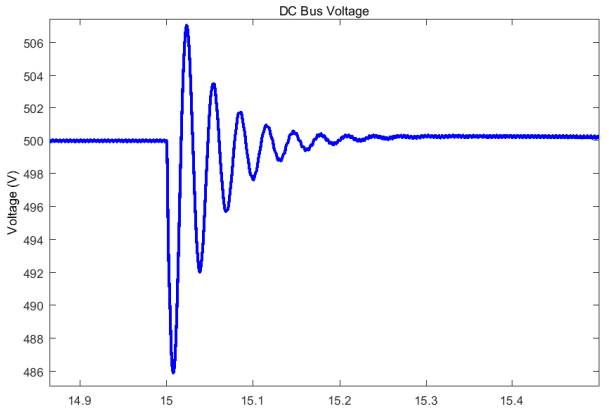

Figure 22. DC link voltage.

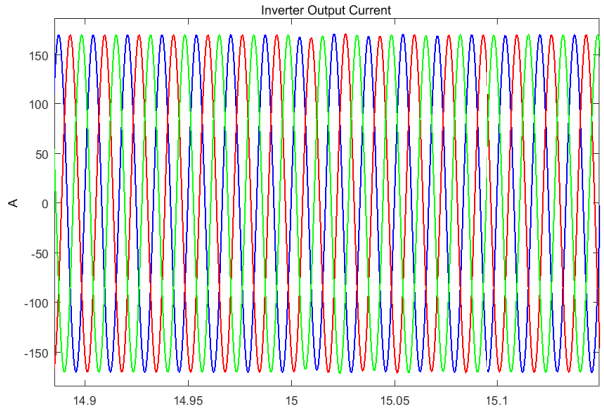

Figure 23. Output current from the inverter.

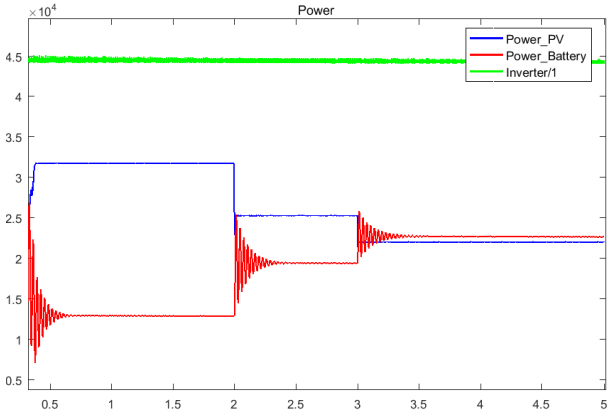

Figure 24. Power exchange in the system.

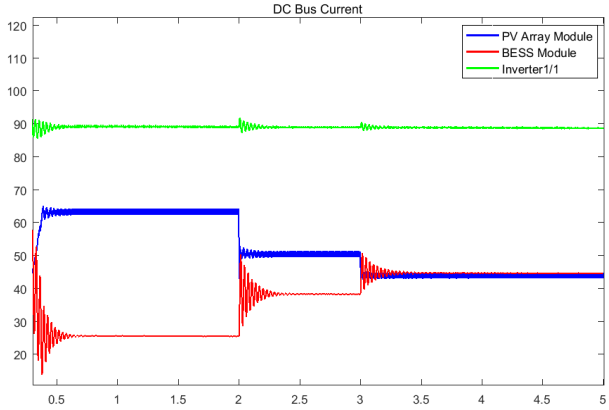

Figure 25. DC link current flows.

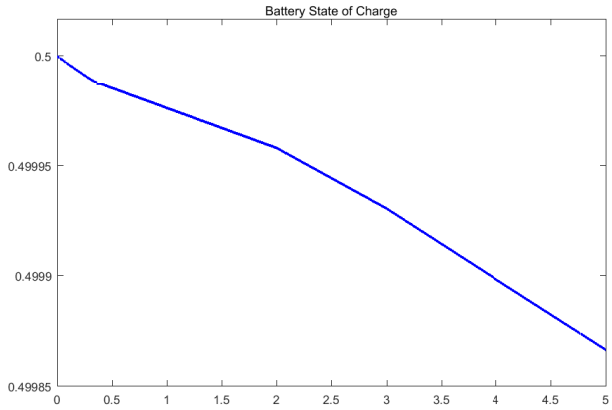

Figure 26. Battery state of charge.

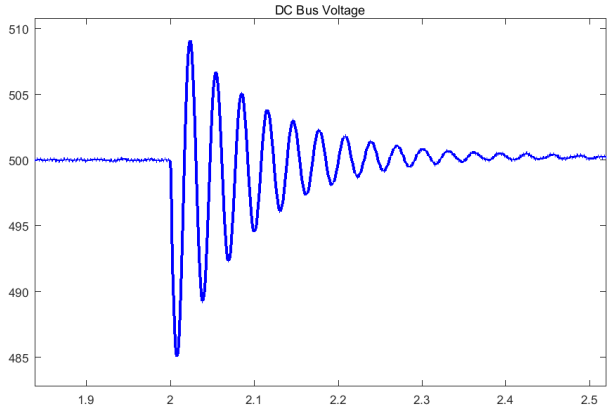

Figure 27. DC link voltage.

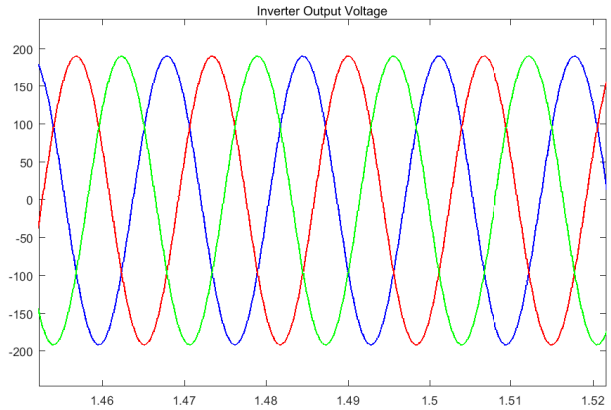

Figure 28. Output voltage from the inverter.

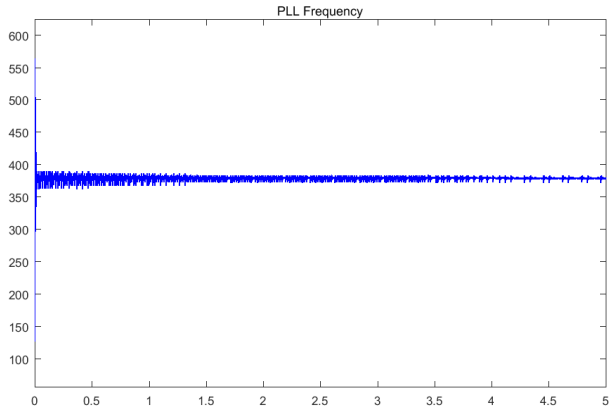

Figure 29. PLL frequency measurement.

the following figures. The power balance condition is similar to the previous case. The battery compensate the demanded power to meet the load demand. The microgrid frequency and voltage is regulated by the DER at desired value, i.e., 60 Hz and 220 V (Line to Line), respectively.

4.1 Power Balance Equation

In a microgrid, the balance between energy production and consumption must be met at each time. The power balance equation and its derivatives without considering the line impedance can be denoted by

$$\Delta P = \sum_{i \in N_G} P_{G_i} + \sum_{i \in N_M} P_{M_i} + \sum_{i \in N_L} P_{L_i} + \sum_{i \in N_W} P_{W_i} + \sum_{i \in N_E} P_{E_i} \tag{31}$$

$$\Delta \dot{P} = \sum_{i \in N_G} \dot{P}_{G_i} + \sum_{i \in N_M} \dot{P}_{M_i} + \sum_{i \in N_L} \dot{P}_{L_i} + \sum_{i \in N_W} \dot{P}_{W_i} + \sum_{i \in N_E} \dot{P}_{E_i} \tag{32}$$

where ΔP is the unbalance power, P_G is the absorbed power from the grid, P_M stands for micro-turbine power, P_W is wind power, P_E denotes the power supply from electrical storage and P_L is the electrical load. For the case that microgrid is connected to the main grid, P_G compensates the unbalanced power mainly via primary frequency control and by using a feedback of ΔP. In case of islanded microgrid, controllable devices such as micro-turbines and storage systems can be used to compensate the mismatched power. Dynamic model of gas micro-turbines consisting of mechanical, combustion, and electrical dynamics can be found in Rowen [1983].

4.2 Load Dynamics

Accurate aggregated load dynamics can be modeled by the Uhlenbeck-Ornstein model as follows:

$$dP_{L_i}(t) = \alpha_L(\bar{P}_L - P_L)dt + \sigma_L dW(t) \tag{33}$$

where $\bar{P}_L$ is a given load profile, α_L is the tracking coefficient and σ_L denotes the variation coefficient. This type of load model can stand for building equipment, electrical heaters and so forth. Uhlenbeck-Ornstein processes have already been used in Weron et al. [2001] to model the deseasonalized data from the California power market and performing out-of-sample forecasts.

4.3 Wind Turbine Dynamics

A wind turbine model can be described as a deterministic system with a stochastic input and can be written as

$$dP_W = \frac{3}{2}\rho R^2 \nu^2 C_p(\eta,\theta)\frac{d\nu}{dt} + \frac{1}{2}\rho R^2 \nu^3 \frac{dC_p(\eta,\theta)}{dt} \tag{34}$$

$$\frac{dC_p(\eta,\theta)}{dt} = \frac{dC_p}{d\eta}.\frac{d\eta}{dt} + \frac{dC_p}{d\theta}.\frac{d\theta}{dt} \tag{35}$$

where ρ is the density, R is the blade radios, ν denotes the stochastic wind speed and C_p refers to efficiency function depending on wind direction (θ) and parameter η. The above wind turbine model is deterministic. However, it is affected by stochastic wind speed ν which can be expressed by the following SDE Strelec et al. [2012].

$$d\nu(t) = -\frac{\nu(t)-\bar{\nu}(t)}{T}dt + k\bar{\nu}(\frac{2}{T})^{0.5}dW(t) \tag{36}$$

where $\bar{\nu}$ is the hourly average of wind speed, the parameter $T = L\bar{\nu}^{-1}$ where L is the turbulence length scale and k is a constant factor. Higher order SDEs can also be used to obtain a better approximation of wind speed.

4.4 Storage Dynamics

A simplified first-order storage model has been considered as follows

$$\frac{dP_S}{dt} = -\eta P_E - P_{Loss}, \quad 0 < \eta < 1 \tag{37}$$

where P_s is the level of stored electrical energy, P_E is the power absorbed/injected to the grid, P_{Loss} denotes a constant stored energy degradation in the sampling interval and η is the power exchange efficiency which is different during charging and discharging mode Parisio et al. [2014].
These type of modelings are more appropriate for slow time scale dynamics (e.g., several minutes or hours) which are more related to energy management systems (EMS) and 24-hours forecast. In this framework, usually longterm response is weakly dependent on fast transient behaviors. As a result, fast dynamics of inverters and other power electronic interfaces can be ignored in the modeling of microgrids.

4.5 Short-Time Scale Photovoltaic Model

Real-time predictions of solar irradiance and power are necessary for designing optimal controllers to better improve the stability, reliability, and efficiency of microgrids. Previous attempts to model solar irradiance can be classified into three general types: physical, frequency distribution and stochastic. Stochastic models are more flexible having the ability to incorporate any non-deterministic influences such as cloud movement and pollution levels into the model, and any non-standard features such as shading specific to a particular location Craggs et al. [1999]. Thus, stochastic prediction is capable for capturing the intrinsically non-deterministic (uncertain) nature of irradiance fluctuations. Understanding the sub-minute

behavior of photovoltaic generation will be necessary to develop realistic predictive models of small microgrids on the order of single houses to single buildings.

In this section, we propose to use a filter-based expectation maximization algorithm and Kalman filter for real-time prediction of solar irradiance and power. This scheme results in a finite dimensional filter which only uses the first and second order statistics. The algorithm is recursive allowing the irradiance and power to be predicted online from received irradiance and power measurements. The algorithms are tested using PV measurement irradiance and power data collected from PV cells located on the roof of the Distributed Energy Communication & Control (DECC) Lab at ORNL. We propose to model the solar irradiance (or power) by the following discrete-time stochastic linear time-variant state-space model

$$\begin{aligned} \vec{x}_{k+1} &= A_k \vec{x}_k + B_k \vec{w}_k \\ \vec{y}_k &= C_k \vec{x}_k + D_k \vec{v}_k \end{aligned} \tag{38}$$

where subscript $k \in \{0, 1, 2, \ldots\}$, $\vec{x}_k$ is a discrete-time state vector, $\vec{y}_k$ is a discrete-time solar irradiance (or power) measurement vector, and $\vec{w}_k$ and $\vec{v}_k$ are the discrete-time state noise and measurement noise respectively. The noise processes $\vec{w}_k$ and $\vec{v}_k$ are assumed to be independent, zero mean, and unit variance Gaussian processes. The unknown system parameters $\theta_k = \{A_k, B_k, C_k, D_k\}$ and the system states $\vec{x}_k$ are unknown and estimated through received signal measurement data, $\vec{y}_n = \{y_1, y_2, \ldots, y_n\}$. The parameters are identified using a filter-based EM algorithm and the channel states are estimated using the Kalman filter. The Kalman filter is introduced next.

4.5.1 Channel State Estimation: The Kalman Filter

The Kalman filter estimates the channel states $\vec{x}_k$ for given system parameter θ_k and measurements $\vec{y}_k$. It is described by the following equations Bishop and Welch [2001]

$$\hat{\vec{x}}_{k|k} = A_{k-1}\hat{\vec{x}}_{k-1|k-1} + P_{k|k}C_{k-1}^T D_{k-1}^{-2}\left(\vec{y}_k - C_{k-1}A_{k-1}\hat{\vec{x}}_{k-1|k-1}\right) \tag{39}$$

$$\hat{\vec{x}}_{k|k-1} = A_{k-1}\hat{\vec{x}}_{k-1|k-1} \tag{40}$$

$$\hat{\vec{x}}_{0|0} = m_0 \tag{41}$$

where $k = 0, 1, 2, \ldots, N$, and $P_{k|k}$ is given by

$$\overline{P}_{k|k}^{-1} = P_{k-1|k-1}^{-1} + A_{k-1}^T B_{k-1}^{-2} A_{k-1} \tag{42}$$

$$P_{k|k}^{-1} = C_{k-1}^T D_{k-1}^{-2} C_{k-1} + B_{k-1}^{-2} - B_{k-1}^{-2}\overline{P}_{k|k}A_{k-1}^T B_{k-1}^{-2} P_{k|k-1} = A_{k-1}P_{k-1|k-1}A_{k-1}^T + B_{k-1}^2 \tag{43}$$

where $B_{k-1}^2 = B_{k-1}B_{k-1}^T$ and $D_{k-1}^2 = D_{k-1}D_{k-1}^T$. The model parameters θ_k are estimated using the EM algorithm which is introduced next.

4.5.2 Channel Parameter Estimation: The EM Algorithm

The filter-based EM algorithm uses a bank of Kalman filters to yield a maximum likelihood (ML) parameter estimate of the Gaussian state space model Elliott and Krishnamurthy [1999]. The EM algorithm is an iterative numerical algorithm for computing the ML estimate. Each iteration consists of two steps: the

expectation and the maximization steps Wu [1983]. The filtered expectation step only use filters for the first and second order statistics. The memory costs are modest and the filters are decoupled and hence easy to implement in parallel on a multi-processor system Elliott and Krishnamurthy [1999]. The algorithm yields parameter estimates with nondecreasing values of the likelihood function, and converges under mild assumptions Wu [1983].

Let $\theta_k = \{A_k, B_k, C_k, D_k\}$ denote the system parameters in (38) and $\{P_{\theta_k} : \theta_k \in \Theta\}$ denotes a family of probability measures induced by the system parameters θ_k. The EM algorithm computes the ML estimate of the system parameters θ_k, given the data $\vec{y}_k$. The expectation step evaluates the conditional expectation of the log-likelihood function given the complete data as

$$\Lambda(\theta_k, \hat{\theta}_k) = E_{\hat{\theta}_k}\left\{\log \frac{dP_{\theta_k}}{dP_{\hat{\theta}_k}} | \vec{y}_k\right\} \tag{44}$$

where $\hat{\theta}_k$ denotes the estimated system parameters at time step k and $E(\cdot)$ is the expectation operator. The maximization step finds

$$\hat{\theta}_{k+1} \in \arg\max_{\theta_k \in \Theta} \Lambda\left(\theta_k, \hat{\theta}_k\right) \tag{45}$$

The expectation and maximization steps are repeated until the sequence of model parameters converge to the real parameters. The EM algorithm is described by Elliott and Krishnamurthy [1999]

$$\begin{aligned}
\hat{A}_k &= E\left(\sum_{i=1}^{k} \vec{x}_i \vec{x}_{i-1}^T | Y_k\right)\left[E\left(\sum_{i=1}^{k} \vec{x}_i \vec{x}_i^T | Y_k\right)\right]^{-1} \\
\hat{B}_k^2 &= \frac{1}{k} E\left(\sum_{i=1}^{k} \left(\left(\vec{x}_i - A_{i-1}\vec{x}_{i-1}\right)\left(\vec{x}_i - A_{i-1}\vec{x}_{i-1}\right)^T\right) | Y_k\right) \\
\hat{C}_k &= E\left(\sum_{i=1}^{k} \vec{y}_i \vec{x}_i^T | Y_k\right)\left[E\left(\sum_{i=1}^{k} \vec{x}_i \vec{x}_i^T | Y_k\right)\right]^{-1} \\
\hat{D}_k^2 &= \frac{1}{k} E\left(\sum_{i=1}^{k} \left(\left(\vec{y}_i - C_{i-1}\vec{x}_i\right)\left(\vec{y}_i - C_{i-1}\vec{x}_i\right)^T\right) | Y_k\right)
\end{aligned} \tag{46}$$

The system (46) gives the EM parameter estimates at each iteration for the model (38). Furthermore, since $\Lambda(\theta_k, \hat{\theta}_k)$ is continuous in both θ_k and $\hat{\theta}_k$, the EM algorithm converges to a stationary point in the likelihood surface Elliott and Krishnamurthy [1999], Wu [1983]. The system parameters $\left\{\hat{A}_k, \hat{B}_k^2, \hat{C}_k, \hat{D}_k^2\right\}$ can be computed from the following conditional expectations Charalambous and Logothetis [2000]

$$\begin{aligned}
L_k^{(1)} &= E\left\{\sum_{i=1}^{k} \vec{x}_i^T Q \vec{x}_i | Y_k\right\} \\
L_k^{(2)} &= E\left\{\sum_{i=1}^{k} \vec{x}_{i-1}^T Q \vec{x}_{i-1} | Y_k\right\} \\
L_k^{(3)} &= E\left\{\sum_{i=1}^{k} \left[\vec{x}_i^T R \vec{x}_{i-1} + \vec{x}_{i-1}^T R^T \vec{x}_i\right] | Y_k\right\} \\
L_k^{(4)} &= E\left\{\sum_{i=1}^{k} \left[\vec{x}_i^T S \vec{y}_i + \vec{y}_i^T S^T \vec{x}_i\right] | Y_k\right\}
\end{aligned} \tag{47}$$

where Q, R, and S are given by

$$Q = \left\{ \frac{e_i e_j^T + e_j e_i^T}{2} \right\} \tag{48}$$

$$R = \left\{ \frac{e_i e_j^T}{2} \right\} \tag{49}$$

$$S = \left\{ \frac{e_i}{2} \right\} \tag{50}$$

for all $i, j \in \{1, 2, \ldots, 2n\}$ in which e_i is the unit vector in the Euclidean space; that is $e_i = 1$ in the i^{th} position and $e_i = 0$ elsewhere. For instance consider the case $2n = 2$, then

$$E\left(\sum_{i=1}^{k} \vec{x}_i \vec{x}_{i-1}^T | Y_k \right) = \begin{bmatrix} L_k^{(3)}(R_{11}) & L_k^{(3)}(R_{12}) \\ L_k^{(3)}(R_{21}) & L_k^{(3)}(R_{22}) \end{bmatrix} \tag{51}$$

where

$$R_{ij} = \left\{ \frac{e_i e_j^T}{2} : i, j = 1, 2 \right\} \tag{52}$$

The other terms in (46) can be computed similarly from (47). The conditional expectations $\left\{ L_k^{(1)}, L_k^{(2)}, L_k^{(3)}, L_k^{(4)} \right\}$ are estimated from the measurements Y_k as described in Olama et al. [2009].

4.5.3 Simulation Results

In this section, the EM algorithm and the Kalman filter is used to predict the solar irradiance and power from PV measurement irradiance and power data collected from PV cells located on the roof of the DECC Lab at ORNL. The collected irradiance $[W/m^2]$ and power data [W] are sampled at one sample per second (sampling rate is 1 Hz). Figure 30 shows one sample irradiance prediction performance for a 4^{th} order model. It can be noticed that the irradiance has been predicted with very high accuracy. It takes a few iterations (about 5 iterations) for the prediction algorithm to converge. The prediction error is shown in Figure 31.

Figure 32 shows the one sample power prediction performance for a 4^{th} order model and its corresponding error. Figure 33 shows the error between the actual power output and the predicted power output for the 4^{th} order model.

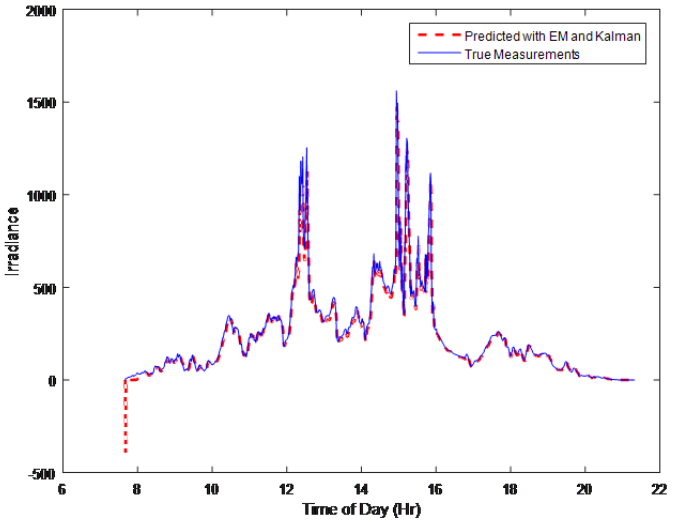

Figure 30. Simulation Results illustrating the performance of the developed EM algorithm together with the Kalman filter in predicting solar irradiance.

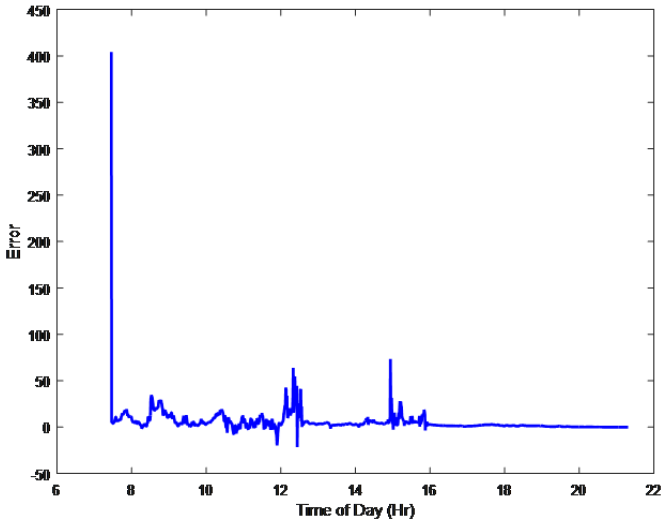

Figure 31. Simulation Error of the developed EM algorithm together with the Kalman filter in predicting solar irradiance.

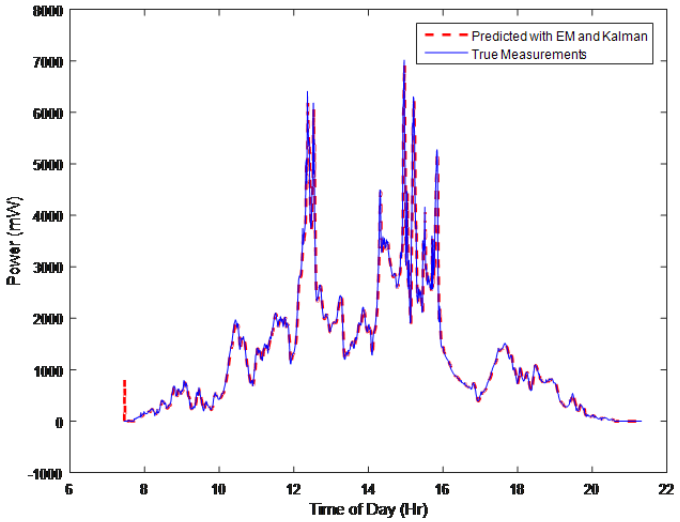

Figure 32. Simulation Results illustrating the performance of the developed EM algorithm together with the Kalman filter in predicting solar power.

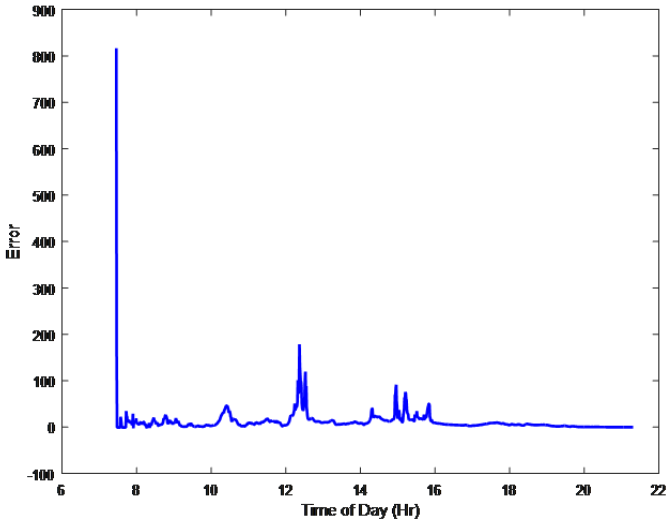

Figure 33. Simulation Error of the developed EM algorithm together with the Kalman filter in predicting solar power.

5. CONTROL FRAMEWORK

Many different control frameworks have been developed to improve the dynamic response and uncertainty tolerance of physical systems. Beginning in the first half of the 20th century with frequency domain techniques and proportional-integral-derivative (PID) control to model stochastic control techniques,control systems have evolved to solve increasingly difficult problems by including nonlinearities in the system dynamics, robust behavior to uncertainties, multiple correlated inputs and outputs, optimization, and stochastic variables.

Microgrids contain many stochastic generations systems, nonlinearities in the system dynamics, and the need to optimize behavior over a wide range of time scales and circumstances. Microgrids and systems of multiple microgrids will need to coordinate and control and coordinate many devices that are geographically isolated with limited communication between devices. These requirements suggest the use of distributed stochastic model predictive control as the framework for microgrid control. In this section the basic frameworks for model predictive control (MPC), stochastic control, and distributed control will be presented, then combined into a novel distributed stochastic model predictive control (dsMPC) framework.

5.1 Model Predictive Control

Model predictive control is commonly used to control large complex industrial systems with slow dynamics such as chemical process systems. Model Predictive Control is a discrete time control system that is designed to optimize the system response over a finite time-horizon. Once the optimal path over the time horizon is calculated, the optimal control action is implemented for the next time period. Then the time horizon is shifted by one period and the process is repeated.

For linearized, discrete-time, state-space models of the system dynamics given by

$$\vec{x}[k+1] = A\vec{x}[k] + B\vec{u}[k] \tag{53}$$

$$\vec{y}[k] = C\vec{x}[k] \tag{54}$$

where $\vec{x} \in \mathbb{R}^n$ is the system state vector, $\vec{u} \in \mathbb{R}^l$ is the command input vector, and $\vec{y} \in \mathbb{R}^m$ is the measured outputs of the system that will be controlled. Based on the formulation given by Maciejowski [2002], the objective of the control is to

i) Obtain the measurements $\vec{y}[k]$

ii) Compute the optimal plant input $\vec{u}[k]$

iii) Apply $\vec{u}[k]$ to the plant

A reference trajectory $\vec{r}[k+i|k]$ will be supplied by the user to describe the ideal behavior of the system. The controller will attempt to force the system states $\vec{x}[k] \rightarrow \vec{r}[k]$ through the control input $\vec{u}[k]$. The future states of the system cannot be measured, so they will be estimated using the discrete-time state-space model. The estimated states are denoted by $\hat{x}[k+i|k]$. Similarly, we will define an optimal control input $\Delta\hat{u}[k+1|k]$ where $\Delta\hat{u}[k+1|k] = \hat{u}[k+1] - \vec{u}[k]$. To add flexibility to the optimization and reduce computational cost, the optimization is performed over finite time horizons given by $i \in [H_w, H_p]$ and $j \in [0, H_u - 1]$ where $H_w \in \mathbb{Z}$, $H_p \in \mathbb{Z}$, and $H_u \in \mathbb{Z}$. Finally, the cost function to be optimized is most

commonly, the scalar valued quadratic cost function given by

$$V[k] = \sum_{i=H_w}^{H_p} Q[i]\|\hat{x}[k+i|k] - \vec{r}[k+i|k]\|^2 + \sum_{j=0}^{H_u-1} R[j]\|\Delta\hat{u}[k+1|k]\|^2 \tag{55}$$

This cost function seeks to minimize the error between the reference state r and the system state x while also minimizing the size of the control effort used $\Delta\hat{u}$.

5.2 Stochastic Control

More recently, in the financial systems, the concept of stochastic control was developed. The fundamental objectives are similar to model predictive control. Model predictive control is designed for deterministic system dynamics, while stochastic control is designed to control systems with stochastic states and outputs. This means that moving a system state from one value to another is no longer valid. Instead, the objective is to maximize the expectation that the system state will be at the final desired value after a period of time.

Another important distinction is the the type of stochastic process. Some processes in a microgrid such as solar generation or load are governed by stochastic differential equations, where the state evolution is a purely stochastic process that is uncontrollable. Other stochastic systems include deterministic components and include the ability to affect the system states through an external input with a stochastic noise component.

In general, stochastic differential equations can be defined as follows:

$$d\vec{x}(t) = b(t, \vec{x}(t))dt + \sigma(t, \vec{x}(t))dW(t), \quad \vec{x}(0) = \vec{x}_0, t \in I \tag{56}$$

where $b : \mathbb{R}^+ \times \mathbb{R}^n \to \mathbb{R}^n$ denotes the drift, $\sigma : \mathbb{R}^+ \times \mathbb{R}^n \to \mathbb{R}^{n\times m}$ denotes the diffusion parameter, and W is a Wiener process that is a non-stationary stochastic process.

This can be expressed as a discrete-time stochastic differential equation given by

$$\vec{x}[k+1] - \vec{x}[k] = \int_k^{k+1} \mu(\vec{x}[s], s)ds + \int_k^{k+1} \sigma(\vec{x}[s], s)dW_s \tag{57}$$

where the first integral is an ordinary Lebesgue integral and the second integral is an Itô integral.

On the other hand a deterministic nonlinear differential equation with stochastic noise such as inverter dynamics can be formulated as Kendrick [2002]

$$\vec{x}[k+1] = f(\vec{x}[k], \vec{u}[k], \vec{w}[k]) \tag{58}$$

$$\vec{y}[k] = h(\vec{x}[k], \vec{v}[k]) \tag{59}$$

where $\vec{w}[k]$ and $\vec{v}[k]$ are generally zero mean Gaussian processes which are stationary processes. This stationary characteristic means that the system states $\vec{x}$ can be estimated without the use of the expectation operator.

When applied to power flow equations, the power balance will be a combination of both stochastic differential equations and deterministic differential equations with stochastic noise terms.

The typical quadratic cost function used with stochastic control is a variation on the cost function used with standard linear MPC algorithms. This optimization has been applied to the deterministic form of the nonlinear differential equations with Gaussian stochastic processes and the cost function is given by

$$V[k] = \vec{E}\left[\sum_{i=H_w}^{H_p} (\hat{x}[k+i] - \vec{r}[k+i])^T Q[i](\hat{x}[k+i] - \vec{r}[k+i]) + \sum_{j=0}^{H_u-1} R[j]\|\Delta\hat{u}[k+1]\|^2\right] \tag{60}$$

which is identical to (55) except for the expectation operator $\vec{E}[\cdot]$.

Functionally, when applied to a microgrid or networked microgrids, this optimization will occur at the device level and the reference signals $\vec{r}[k]$ will be supplied another optimization that will attempt to optimize the overall behavior of the microgrids for different desired behaviors like load flattening or maximizing efficiency. This separation of duties leads to a natural breakup of control functionality into different scales and devices which is what distributed control is designed to accomplish.

5.3 Distributed Control

Distributed control came to prominence with the advent of multiagent systems. These systems need to coordinate their behavior across time and spatial domains with limited communications and computation. Coordination among agents lead to “complex optimization problems that need to be solved in a scalable manner Ahmed et al. [2016]." An agreed upon definition of distributed control does not seem to exist. Rather, control architectures are classified based on the amount of computation that occurs at the edges (centralized, hierarchical, distributed, or some combination). Often the choice of architecture is highly dependent on the specific system being controlled because of limitation on computation power and communication. Distributed controls do not provide the performance of centralized controllers although they can approach it, but distributed control “provide better scalability, naturally parallelized computation, and resilience to communication loss and hardware failure Ahmed et al. [2016]." This scalability will be critical for coordinating the power grid as more stochastic generation sources are added. As an example, if only 1% of the american population added solar panels, batteries, and an inverter to their houses, this would be more than *3 million* new devices that need to be coordinated to maintain the stability of the power grid.

To understand distributed controls, we will develop a simplified mathematical formulation of a linear coupled distributed control system given in van Schuppen [2011] known as a *distributed Gaussian system* that consists of two nodes with the node 1 dynamics given by

$$\vec{x}_1[k+1] = A_{11}\vec{x}_1[k] + B_1\vec{u}_1[k] + B_{12}\vec{u}_{12}[k] \tag{61}$$
$$\vec{y}_1[k] = C_1\vec{x}_1[k] \tag{62}$$
$$\vec{u}_{21}[k] = C_{21}\vec{x}_1[k] \tag{63}$$

and the node 2 dynamics given by

$$\vec{x}_2[k+1] = A_{22}\vec{x}_2[k] + B_{21}\vec{u}_{21}[k] + B_2\vec{u}_2[k] \tag{64}$$
$$\vec{y}_2[k] = C_2\vec{x}_2[k] \tag{65}$$
$$\vec{u}_{12}[k] = C_{12}\vec{x}_2[k] \tag{66}$$

In this formulation, the matrices B_{12} and B_{21} couple the input to the the state of the two nodes and the matrices C_{12} and C_{21} couple the state of the outputs of the two nodes to each other. The overall system can be converted to the general linear discrete state-space system given by (53). This is done using the combined system vectors given by the state $\vec{x} = [\vec{x}_1, \vec{x}_2]^T$, input $\vec{u} = [\vec{u}_1, \vec{u}_2]^T$, and output $\vec{y} = [\vec{y}_1, \vec{y}_2]^T$ and the basic linear discrete-time differential equation equations

$$\vec{x}[k+1] = A\vec{x}[k] + B\vec{u}[k] \tag{67}$$
$$\vec{y}[k] = C\vec{x}[k] \tag{68}$$
$$\tag{69}$$

By inspection, this yields the system matrices given by

$$A = \begin{bmatrix} A_{11} & B_{12}C_{12} \\ B_{21}C_{21} & A_{22} \end{bmatrix}, \quad B = \begin{bmatrix} B_1 & 0 \\ 0 & B_2 \end{bmatrix} \tag{70}$$
$$C = \begin{bmatrix} C_1 \\ C_2 \end{bmatrix} \tag{71}$$

Similarly, this can be expanded to an n-th order distributed system. The control objective is to design two distributed controllers $\vec{u}_1 = K_1(\vec{y}_1)$ and $\vec{u}_2 = K_2(\vec{y}_2)$ such that the combined system states are stable (i.e. $\lim_{k\to\infty} \vec{x}[k] = 0$).

5.4 Distributed Stochastic Model Predictive Control

Distributed stochastic model predictive control can be considered an extension of both distributed control and stochastic control. We will use a discrete linear Gaussian form of the system similar to the formulation given in van Schuppen [2011]. While this system is two nodes, it can be easily extended to N nodes. Node 1 equations are given by

$$\vec{x}_1[k+1] = A_{11}\vec{x}_1[k] + B_1\vec{u}_1[k] + B_{12}\vec{u}_{12}[k] + M_1\vec{w}[k] \tag{72}$$
$$\vec{y}_1[k] = C_1\vec{x}_1[k] + N_1\vec{v}[k] \tag{73}$$
$$\vec{u}_{21}[k] = C_{21}\vec{x}_1[k] + N_{21}\vec{v}[k] \tag{74}$$

and the node 2 dynamics given by

$$\vec{x}_2[k+1] = A_{22}\vec{x}_2[k] + B_{21}\vec{u}_{21}[k] + B_2\vec{u}_2[k] + M_2\vec{w}[k] \tag{75}$$
$$\vec{y}_2[k] = C_2\vec{x}_2[k] + N_2\vec{v}[k] \tag{76}$$
$$\vec{u}_{12}[k] = C_{12}\vec{x}_2[k] + N_{12}\vec{v}[k] \tag{77}$$

The overall system can be converted to the general linear discrete state-space system given by (53). This is done using the combined system vectors given by the state $\vec{x} = [\vec{x}_1, \vec{x}_2]^T$, input $\vec{u} = [\vec{u}_1, \vec{u}_2]^T$, output $\vec{y} = [\vec{y}_1, \vec{y}_2]^T$, noise vector $\vec{\zeta} = [\vec{w}, \vec{v}]^T$, and the basic linear discrete-time differential equation equations

$$\vec{x}[k+1] = A\vec{x}[k] + B\vec{u}[k] + M\vec{\zeta}[k] \tag{78}$$
$$\vec{y}[k] = C\vec{x}[k] + N\vec{\zeta}[k] \tag{79}$$
$$\tag{80}$$

By inspection, this yields the system matrices given by

$$A = \begin{bmatrix} A_{11} & B_{12}C_{12} \\ B_{21}C_{21} & A_{22} \end{bmatrix}, \quad B = \begin{bmatrix} B_1 & 0 \\ 0 & B_2 \end{bmatrix}, \quad M = \begin{bmatrix} M_1 & N_{12} \\ N_{21} & M_2 \end{bmatrix} \tag{81}$$

$$C = \begin{bmatrix} C_1 \\ C_2 \end{bmatrix}, \quad N = \begin{bmatrix} N_1 \\ N_2 \end{bmatrix} \tag{82}$$

6. CONTROL OBJECTIVE FUNCTIONS

Control requirements for individual microgrids generally fall into two time-scale categories. When analyzing microgrid performance locally, short time-scale objectives revolve around frequency and voltage regulation. When operating in grid-connected mode, voltage regulation is performed at the point of common connection (PCC) by the power grid because of the large inertia existing in the grid compared to the loads and generation sources locally. Currently, when a microgrid operates in island mode, both frequency and voltage regulation (primary and secondary control) are performed by individual localized microgrid controllers or a centralized controller. Voltage and frequency regulation take place at fast time scales that need to operate at sub-cycle speeds (i.e. much faster than 60 Hz). In these instances, the control actions need to stabilize operation on sub-second time scales.

The tertiary control functions currently provided by centralized microgrid controllers happen at much slower time scales on the order of minutes to days. These control functions are concerned with resource planning tasks such as storing enough energy in a battery system to maintain microgrid power for the duration of a storm or smoothing the load seen at the PCC during a 24 hour period. Most work on microgrid control has focused on short time-scale device control and more recently single microgrid planning and device coordination. Far less work has focused on coordination and control of multiple microgrids through tertiary control.

For distribution companies, microgrids are a bit of an enigma when it comes to incorporating them into their distribution architecture. Utilities see microgrids as useful during storm events to prevent power outages because of their islanding capabilities. However, these extreme situations happen only a small fraction of the time so currently in the view of distribution companies, microgrids have limited usefulness. Microgrids though can create new functionalities for utilities during normal operation such as load smoothing which can save them money because of the structure of price agreements with transmission companies that penalize peak power usage by distribution companies.

Beyond the economic benefits to distribution companies and customers from increased reliability and flattened load profiles, microgrids seem to be the only way to enable large concentrations of local generation. Because of the stochastic nature of loads and some distributed generation sources such as solar, regulating voltage and frequency becomes impossible if a high enough concentration of energy used by consumers is created using uncontrollable (non-dispatchable) generation sources like solar. Currently the existing transmission and distribution system in the United States cannot remain stable under these circumstances. However, re-configuring our distribution system architecture as a group of interconnected microgrids with integrated storage should allow high concentrations of distributed generation sources to be deployed in the U.S. making our power grid more resilient to both natural and anthropogenic threats.

An important unsolved technical challenge is to coordinate and control energy generation, storage, and consumption both at the microgrid level and at the distribution level as a collection of networked microgrids. This section is intended to analyze and solve some of these coordination and control problems at the multi-microgrid distribution system level. While the fast time-scale device controller for regulating frequency, voltage, and power injection are important, these topics are sufficiently well researched to be utilized at their current state of technological readiness. See sections 2. and 3. for more information. This research if focused more on the overall coordination and control of multiple microgrids and creating techniques with which they can interact more efficiently to provide new functionality for utility grids and stability with high concentrations of non-dispatchable generation.

First we will develop some objective functions for different types of desired behavior by multiple microgrids that will be used to optimize their performance over a time period.

6.1 Load Flattening

As stated above, distribution companies would like to flatten their load profile over a 24-hour period. From a hardware point of view, this means that a microgrid must have either dispatchable generation available like a propane generator or a combination of non-dispatchable generation that has excess capacity beyond the needs of the microgrid and storage. This is because of the fundamental law that power consumed $P_L(t)$ needs to equal generation $P_g(t)$

$$P_L(t) = P_g(t), \ \forall t \tag{83}$$

When this equality is not valid, transients that can damage electrical equipment are introduced into the system. When dealing with solar panels and other stochastic generation sources, the power created in a time interval $T_k \in [t_k, t_{k+1}]$ is given by

$$E[P_g(T_k)] = \int_{t_k}^{t_{k+1}} \frac{E[P_g(t)]}{t_{k+1} - t_k} \tag{84}$$

Similarly, on the same time interval T_k, the power used is given by

$$E[P_L(T_k)] = \int_{t_k}^{t_{k+1}} \frac{E[P_L(t)}{t_{k+1} - t_k} \tag{85}$$

The difference between these two quantities

$$\Delta P_r(T_k) = E[P_L(T_k)] - E[P_g(T_k)] \tag{86}$$

is the main cause of voltage and frequency fluctuations. Neither of these stochastic quantities are zero mean. Furthermore, while the generation looks like a Gaussian distribution with time varying mean and variance $E[P_g(T_k)] \in N(\mu(T_k), \sigma^2(T_k))$, locally a load distribution looks more like the sum of random binary sequences of different magnitudes. Usually, loads are aggregated over hundreds or thousands of nodes on an individual feeder and act as a similar time varying normal distribution to the generation, but when viewed as a local load source, their random binary nature emerges. This is due to the fact that most loads in a home are dual state (on/off) e.g. light bulbs, stoves, and HVAC systems. In a traditional distribution network this statistical aggregation of loads means that centralized generation sources only need to follow the average time-varying power consumption, however, when the generation is localized, it needs to follow the different statistical distribution of the local loads. *The response of current controller designs to these highly localized non-Gaussian transients have not currently been analyzed theoretically.* Because of this, the maximum concentration of non-dispatchable generation for stable operation is still unknown.

6.1.1 Grid Connected Operation

When the microgrid is connected to the main power distribution network the power received from the grid $P_G(T_k)$ can balance the load and generation, but during islanded mode, the microgrid needs to have either fast dispatchable generation sources $P_N(T_k)$, power storage $P_S(T_k)$, or a combination of both to maintain

the balance between load and generation. This leads to the first constraint that needs to be satisfied by the controls system and optimization

$$E[P_L(T_k)] = E[P_g(T_k)] + P_G(T_k) + P_N(T_k) + P_S(T_k) \tag{87}$$

Also, we will define $E(T_k) = E[P_g(T_k)] - E[P_L(T_k)]$ as the difference between local generation and load on the time interval T_k. Obviously the magnitude of $\|E(T_k)\|$ is highly dependent on the length of the time interval $\|T_k\|$ and the dynamics of the grid, dispatchable generation, and storage. In particularly, if the dynamics of the grid, deterministic generation, and storage sources are such that they cannot quickly respond to real variations in generation and load, the power grid will experience fluctuations in voltage and frequency. This leads to the inequality constraint

$$\max_{t \in T_k} \left(\frac{\mathrm{d}P_L(T_k)}{\mathrm{d}t} - \frac{\mathrm{d}P_g(T_k)}{\mathrm{d}t} \right) > \max \left(\frac{\mathrm{d}P_G(T_k)}{\mathrm{d}t}, \frac{\mathrm{d}P_N(T_k)}{\mathrm{d}t}, \frac{\mathrm{d}P_S(T_k)}{\mathrm{d}t} \right) \tag{88}$$

which is an abuse of notation. Obviously the response speed of the grid, batteries, and dispatchable generation sources are dependent on the physical devices used. This abuse of notation is meant to express the need to think beyond the steady state or maximum capacity capabilities of the deterministic devices used and additionally focus on the transient response of the devices. More subtly, this inequality constraint is a function of the time interval T_k. *This implies that the choice of T_k in the optimization is critical* because at small time intervals, sensor noise is the dominating dynamics in the system and at large values of T_k the dynamics of the difference between generation and load are averaged and no longer capture the short term variations in the error $\Delta P_r(T_k)$ which in turn will cause excessive voltage and frequency deviations.

Of the three generation sources P_G, P_N, and P_S, only the grid power is uncontrollable at the local level. This implies that a planning controller should have algorithms for deciding the values of P_N and P_S in such a way that optimizes the long term stability of the system. This is decidedly easier when the microgrids are connected to the distribution system because the grid can supply excess power to the microgrid. On the other hand, when the grid is in island mode, the generation sources are resource limited and can only supply as much power as is stored in the system when the island mode is activated.

This leads to a number of fundamental problems that need to be addressed by the control and coordination system. First, to be resilient to natural and anthropogenic effects on the grid that cause the microgrid to be operated in island mode, the microgrid needs to be designed with enough storage and generation to meet the load requirements of the microgrid for a period of time greater than it will take to restore service that we will denote as T_res. This is a highly localized value and depends on the resources of the utility and the severity of the damage. The average restoration time is a metric that utilities are required to report, but generally, this is averaged over all customers making it less than optimal for the design of microgrid storage and local generation. On the other hand, their are many utilities such as the Chattanooga Electric Power Board that have highly instrumented their distributions systems and have access to individual household data on average times to fix any physical damage and restore power. Second, effective planning requires accurate prediction algorithms for the expected power that can be generated over a 24-72 hour period. This includes estimation of the likelihood of a severe weather event either through machine learning or human input.

As stated before, there are some long term objectives that the coordination and control system should meet subject to the constraints developed. When a microgrid is connected to the distribution system, one of the primary objectives of the distribution companies is minimizing the overall peak power demand over a

month

$$\min_{T_k=1\,month}\left(\max_{t\in T_k} E[P_G(T_k)]\right) = \min\left(\max_{\forall t\in T_k} E[P_L(t)] - E[P_g(t)] - P_N(t) - P_S(t)\right) \tag{89}$$

which is clearly a stochastic optimization problem due the the two stochastic terms. For the optimization to be feasible over this long time period, the estimation of the statistical distribution parameters of $P_L(t)$ and $P_g(t)$ needs to be accurate or the storage and local dispatchable generation capacities $P_S(t)$ and $P_N(t)$ need to be able to provide local power for a significant portion of the optimization period. Since currently, accurate load prediction capabilities lose accuracy after a few days and deploying such a large generation and storage capacity would be excessively expensive, the suboptimal solution over a 24 hour period will be given by

$$\min_{T_k=24\,hr}\left(\max_{t\in T_k} E[P_G(T_k)]\right) = \min\left(\max_{\forall t\in T_k} E[P_L(t)] - E[P_g(t)] - P_N(t) - P_S(t)\right) \tag{90}$$

will be utilized. Taking advantage of the cyclical nature of power over a 24 hour period and the mathematical equivalency

$$\min\left(\max_{t\in[t_1,t_2]} E[P(t)]\right) = \min_{t\in[t_1,t_2]} E[(P(t) - E[P(t)]^2)] \tag{91}$$

the 24 hour objective function can be described and minimizing the variation in $P_G(t)$ over a 24 hour period which is equivalent to

$$\min_{T_k=24\,hr} E[(P_G(T_k) - E[P_G(T_k)])^2] \tag{92}$$

This implies that the storage and generation are absorbing all the fluctuation about the average power used in a 24 hour period $E[P_L(t)]$, $t \in [0, 24\,hr]$. Taking into account the power limitations of the storage $E_S \in [0, \overline{E_S}]$ and the local dispatchable generation $\int_{t\in T_k} P_G(t)\mathrm{d}t < \overline{E_N}$ where $\bar{\cdot}$ denotes the maximum energy storage capacity of the storage and generation fuel supply respectively. Because the fuel supply for the local generation P_G is limited and has a long lead time for replacement (hours to days), this implies that the local storage should provide the majority of load balancing to be most efficient, resilient, and responsive to reducing variations in load. This leads to the complete optimization problem for minimizing the maximum microgrid load as seen by the utility given by

$$\min_{P_N(t),P_S(t),\ \forall t\in T_k} E[(P_G(T_k) - E[P_G(T_k)])^2] \tag{93}$$

$$sub\,ject\ to \tag{94}$$

$$0 \le E_s \le \overline{E_S} \tag{95}$$

$$\int_0^{T_k} P_N(t)(d)t <= \overline{E_N} \tag{96}$$

where $T_k = 24\,hr$ and $P_G(T_k) = E[P_L(t)] - E[P_g(t)] - P_N(t) - P_S(t)$.

Another objective could be the minimization of the rate of charge and discharge in the battery which is equivalent to maximizing the capacity of the battery.

$$\min \quad \frac{P_S(T_{k+1}) - P_S(T_k)}{k} \tag{97}$$

$$s.t. \tag{98}$$

$$E[P_L(T_k)] = E[P_g(T_k)] + P_N(T_k) + P_S(T_k) \tag{99}$$

6.1.2 Island Mode

Similarly to grid connected operation, load flattening has uses when the microgrid is in island mode. Load flattening in island mode doesn't provide any financial incentives for the distribution company. However, when the microgrid is in island mode, one of the main power sources are the battery storage systems. Battery storage capacity is dependent upon the discharge rate of the batteries and there are additional power losses when charging and discharging the batteries so flattening the load on the battery will improve the total energy available and the efficiency of the microgrid. This is particularly important when in island mode because energy resources are scarce and need to be extended as long as possible.

In island mode, the power balance equation becomes

$$E[P_L(T_k)] = E[P_g(T_k)] + P_N(T_k) + P_S(T_k) \tag{100}$$

Note that without other forms of dispatchable localized generation such as natural gas generators, there is no possibility of meeting the load flattening objective because the storage needed to balance load and generation $P_S(T_k)$

$$P_S(T_k) = E[P_L(T_k)] - E[P_g(T_k)] \tag{101}$$

is a function of two stochastic quantities which makes it a stochastic quantity that is uncontrollable.

This leads to the load flattening objective during island mode given by

$$\min_{T_k=24\,hr} E[(P_S(T_k) - E[P_S(T_k)])^2] \tag{102}$$

However, other objectives than flattening the load that the batteries see during island mode may be important to the operators. For example, minimizing the use of carbon creating generation sources like $P_N(T_k)$ or maximizing the time that the generation sources can supply power to the microgrid in island mode

$$\max_n \sum_{k=0}^{k=n} E[P_L(T_k)] - E[P_g(T_k)] + E[P_N(T_k)] + E[P_S(T_k)] \tag{103}$$

7. CONCLUSION

This report provided a detailed summary of the research accomplished into developing new distributed stochastic control systems for coordination and control of multiple microgrids. Section 2. details the dynamic models of individual system components that are used to understand their dynamic behavior and combine into larger scale coupled system models of microgrids. Section 3. defines the three levels of the control system hierarchy used in literature and examples of the current typical controller designs used in microgrid controllers. Section 4. provides details on the software implementation of the component models combined with primary and secondary controllers. Section 5. develops the fundamental mathematical framework of the proposed distributed stochastic optimal control that will be used as the microgrid controller. Section 6. develops some microgrid controller objective functions that optimize the microgrid behavior during both grid-tied and island mode.

The next steps for this research are the combination of the controller framework and objectives into a functional theoretical framework that can be applied to develop functional microgrid controllers that provide new functionality to both consumers and distribution companies.

8. REFERENCES

N. R. Ahmed, J. Cortes, and S. Martinez. Distributed control and estimation of robotic vehicle networks. *IEEE Control Systems Magazine*, 36(4), 2016.

S Armstrong, ME Glavin, and WG Hurley. Comparison of battery charging algorithms for stand alone photovoltaic systems. In *2008 IEEE Power Electronics Specialists Conference*, pages 1469–1475. IEEE, 2008.

G. Bishop and G. Welch. *An introduction to the Kalman filters*. University of North Carolina, 2001.

Vladimir Blasko and Vikram Kaura. A new mathematical model and control of a three-phase ac-dc voltage source converter. *IEEE transactions on Power Electronics*, 12(1):116–123, 1997.

Mukul C Chandorkar, Deepakraj M Divan, and Rambabu Adapa. Control of parallel connected inverters in standalone ac supply systems. *IEEE Transactions on Industry Applications*, 29(1):136–143, 1993.

C.D. Charalambous and A. Logothetis. Maximum-likelihood parameter estimation from incomplete data via the sensitivity equations: The continuous-time case. *IEEE Transaction on Automatic Control*, 45(5), 2000.

C. Craggs, E. Conway, and N. M. Pearsall. Stochastic modelling of solar irradiance on horizontal and vertical planes at a northerly location. *Renewable Energy*, 18(4), 1999.

R.J. Elliott and V. Krishnamurthy. New finite-dimensional filters for parameter estimation of discrete-time linear guassian models. *IEEE Transaction On Automatic Control*, 44(5), 1999.

Qiang Fu. Modeling, analyses and assessment of microgrids considering high renewable energy penetration. Master's thesis, University of Wisconsin-Milwaukee, 2013.

Hua Han, Xiaochao Hou, Jian Yang, Jifa Wu, Mei Su, and Josep M Guerrero. Review of power sharing control strategies for islanding operation of ac microgrids. *IEEE Transactions on Smart Grid*, 7(1): 200–215, 2016.

D. A. Kendrick. *Stochastic Control for Economic Models*. McGraw-Hill, 2002.

Xiong Liu, Peng Wang, and Poh Chiang Loh. A hybrid ac/dc microgrid and its coordination control. *IEEE Transactions on Smart Grid*, 2(2):278–286, 2011.

J. M. Maciejowski. *Predictive Control with Constraints*, chapter A basic formulation of predictive control. Pearson, 2002.

E Muljadi, M Singh, and B Gevorgian. Pscad modules representing pv generator. Technical report, National Renewable Energy Laboratory (NREL), 2013.

M. M. Olama, S. M. Djouadi, and C. D. Charalambous. Stochastic differential equations for modeling, estimation and identification of mobile-to-mobile communication channels. *IEEE Transactions on Wireless Communications*, 8(4), 2009.

Daniel E Olivares, Ali Mehrizi-Sani, Amir H Etemadi, Claudio A Cañizares, Reza Iravani, Mehrdad Kazerani, Amir H Hajimiragha, Oriol Gomis-Bellmunt, Maryam Saeedifard, Rodrigo Palma-Behnke, et al. Trends in microgrid control. *IEEE Transactions on smart grid*, 5(4):1905–1919, 2014.

A. Parisio, E. Rikos, and L. Glielmo. A model predictive control approach to microgrid operation optimization. *IEEE Transactions on Control Systems Technology*, 22, 2014.

Joan Rocabert, Alvaro Luna, Frede Blaabjerg, and Pedro Rodriguez. Control of power converters in ac microgrids. *IEEE Transactions on Power Electronics*, 27(11):4734–4749, 2012.

I. Rowen. Simplified mathematical representations of heavy-duty gas-turbines. *Journal of Engineering for Power*, 105, 1983.

Qobad Shafiee, Josep M Guerrero, and Juan C Vasquez. Distributed secondary control for islanded microgridsâĂŤa novel approach. *IEEE Transactions on power electronics*, 29(2):1018–1031, 2014.

M. Strelec, K. Macek, and A. Abate. Modeling and simulation of a microgrid as a stochastic hybrid system. In *IEEE PES International Conference on Innovative Smart Grid Technologies*. IEEE, 2012.

Olivier Tremblay and Louis-A Dessaint. Experimental validation of a battery dynamic model for ev applications. *World Electric Vehicle Journal*, 3(1):1–10, 2009.

Olivier Tremblay, Louis-A Dessaint, and Abdel-Illah Dekkiche. A generic battery model for the dynamic simulation of hybrid electric vehicles. In *Vehicle power and propulsion conference, 2007. VPPC 2007. IEEE*, pages 284–289, 2007.

J. H. van Schuppen. Control of distributed stochastic systems - introduction, problems, and approaches. In *IAFC World Congress*. IAFC, 2011.

Marcelo Gradella Villalva, Jonas Rafael Gazoli, et al. Comprehensive approach to modeling and simulation of photovoltaic arrays. *IEEE Transactions on Power Electronics*, 24(5):1198–1208, 2009.

Xiaoyu Wang, Meng Yue, and Eduard Muljadi. Modeling and control system design for an integrated solar generation and energy storage system with a ride-through capability. In *2012 IEEE Energy Conversion Congress and Exposition (ECCE)*, pages 3727–3734. IEEE, 2012.

R. Weron, B. KozÅĆowska, , and J. Nowicka-Zagrajek. Modeling electricity loads in california: a continuous-time approach. *Physica A: Statistical Mechanics and its Applications*, 299, 2001.

C.F.J. Wu. On the convergence properties of the em algorithm. *Annals of Statistics*, 11, 1983.

A Yafaoui, B Wu, and R Cheung. Implementation of maximum power point tracking algorithm for residential photovoltaic systems. In *2nd Canadian solar buildings conference Calgary*, pages 10–14, 2007.

Mehrdad Yazdanian and Ali Mehrizi-Sani. Distributed control techniques in microgrids. *IEEE Transactions on Smart Grid*, 5(6):2901–2909, 2014.